Article

# Enhancing SERS Spectra through Surface-Doped Nanocluster Substrates: A Numerical Investigation of Plasmonic Silver Coated Pt and Pd Core−Shell-Satellite Structures

Patrick Irigo, Nada Yousif, Ian Johnston, Boyan Tatarov, Avinash Yadav, Etelka Chung, Kun Luo, and Guogang Ren*

Read Online

ACCESS | Metrics & More | Article Recommendations

**ABSTRACT:** This study numerically investigates the design and function of single bifunctional entities that integrate catalytic activity (Pd/Pt) and Surface-Enhanced Raman Spectroscopy (SERS) activity (Ag). Our approach aims to construct multilayered plasmonic structures with abundant electromagnetic hotspots for sensitive biomolecule detection. By synthesizing complex hybrid metal nanostructures, we aim to overcome limitations in monitoring catalytic reactions, ensuring simultaneous high SERS activity and a large surface area of the catalytically active metal. Utilizing finite-difference time-domain analysis, we evaluate Ag@ Pd/Pt@Ag plasmonic core−shell-satellite (PCSS) nanostructures (100 nm core, 2−3 nm shell, 10−30 nm satellites). The pyramidal configuration, featuring a Pd shell demonstrates superior electric field enhancement (approximately $10^9$), offering valuable insights into the synergistic interplay of transition metal nanospacers and satellite nanoclusters in PCSS structures. This study contributes to advancing the understanding of nanotechnology and spectroscopy, aiming to develop robust and cost-effective PCSS nanostructures for reliable sensing applications and theoretical advancements in engineering.
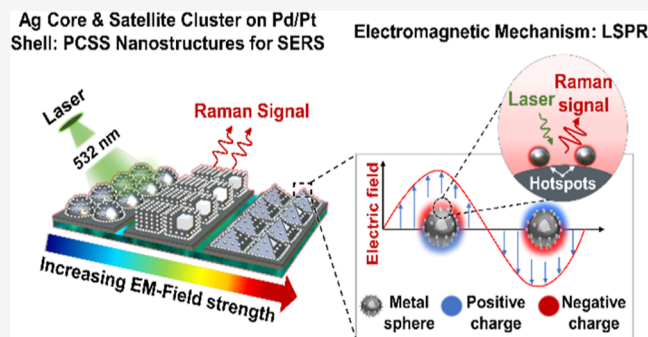
## INTRODUCTION

Surface-Enhanced Raman Spectroscopy (SERS) is a novel high-sensitivity spectral analysis technique frequently employed for detecting substances at ultralow concentrations, even at the single molecule level.[1] SERS offers accurate spectral "fingerprint" data for samples, leveraging its exceptional sensitivity, selectivity, and minimal susceptibility to interference from water or fluorescence, thereby facilitating rapid analytical detection of drugs and biological substances.[2] In the biomedical field, SERS emerges as a potent analytical method,[3] providing enhanced Raman signals for precise molecular exploration in medicine and life sciences.[4] Its distinct capability to amplify signals from target molecules such as antibiotics (e.g., ciprofloxacin, fluoroquinolones) and biomarkers (e.g., miRNA) facilitates sensitive and precise disease diagnostics.[5] Additionally, SERS finds applications in bacterial sensing,[6] biological imaging,[7] environmental monitoring,[8] food safety,[9] and forensic science,[10] offering innovative solutions across these fields.

The enhancement of signals in SERS-active substrates hinges on the creation of electromagnetic (EM) "hotspots".[11] These "hotspots" represent localized areas characterized by significantly heightened electric field intensity surrounding metallic nanoparticles (NPs), which exceed the strength of the incident field. The excitation of localized surface plasmon resonance (LSPR) in plasmonic NPs, especially at geometric vertices and nanogaps, contributes to the formation of intense "hotspots".[12] LSPR is a fascinating optical phenomenon that occurs when conductive plasmonic NPs with dimensions smaller than the incident wavelength interact with light giving rise to plasmons, which locally oscillate around each individual metal NP seen in Figure 1i. In contrast to conventional SPR, which takes place at the interface between conducting materials and dielectrics, LSPR is confined to nanoscale regions, typically occurring near or directly at the surface of NPs.[13] The frequency of these plasmonic oscillations is referred to as the LSPR frequency.[14] This confined resonance phenomenon offers unique optical
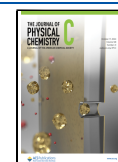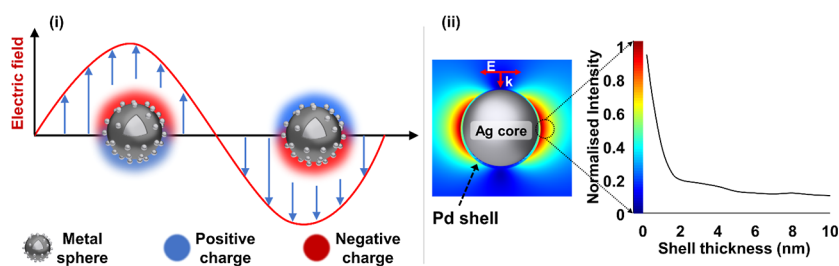
**Figure 1.** (i) Visualization of plasmon oscillation: displacement of conduction electron gas in a spherical metal NP. (ii) finite-difference time-domain (FDTD) simulation illustrating the distribution of the EM-field in Ag@Pd NPs (left). Correlation between EM intensity (normalized) and Pd shell thickness (right).

properties and is a consequence of the interaction between incident light and NPs, making it a vital analytical tool.

The generation and intensity of EM "hotspots" are influenced by three key factors: the structural[15] and optical properties[16] of the NPs and the matching wavelength of the incident light.[17] The "hotspots" observed on NPs, commonly linked with LSPR, represent intriguing nanoscale phenomena that have recently garnered considerable research.[18] The "hotspots" can generate a SERS signal enhancement factor (EF) as large as $10^{11}$ for analytes placed in the area (1−10 nm).[19] Prior studies have explored the utilization of EM "hotspots" in SERS detection, including their application in plasmonic arrays and quantum dot semiconductors to enhance sensing. By carefully organizing these "hotspots", researchers have achieved simultaneous and swift detection of multiple analytes.[20] This makes plasmonic "hotspot" arrays valuable tools for multiplexed detection, enabling the detection of diverse analytes in a single assay.

The optimum SERS-active substrate must be durable, easily fabricated and deliver a consistent and reproducible signal enhancement. As previously discussed, developing, and optimizing the SERS substrate relies on several structural/physical factors such as its dimensions,[21] precise edges,[22] apexes,[23] surface texture,[24] and nanogap distances.[25] Bare AgNPs are widely used in SERS applications but suffer from limited sensitivity, stability, and reproducibility, particularly when it comes to plasmonic absorption at longer wavelengths.[26] To further expand SERS substrate applications, ultrathin shells, comprising transition metals (Pt, Pd, and Ru) and nonmetals ($SiO_2$, $TiO_2$, $Al_2O_3$, graphene), can shield the core, thereby preventing interference from analyte molecules and the environment.[27,28,29,30,31] Transition metal nanoshells primarily use the "borrowing SERS activity" strategy proposed and documented by Van Duyne and colleagues in 1983, to overcome the limitations associated with nonplasmonic SERS materials.[32] This strategy involves leveraging the enhanced EM field generated by adjacent plasmonic NPs, which significantly amplifies the Raman signals of nearby nonplasmonic molecules.

This SERS enhancement approach can be validated by analyzing the distribution and intensity of the electric field using the FDTD approach illustrated in Figure 1. Pt and Pd, known for stability[33] and biocompatibility[34] enhance SERS signals, making them advantageous for combined SERS and catalytic applications.[35] For optimal SERS signals, maintaining an ultrathin shell (1−3 nm) is recommended for the proximity of probe molecules to the plasmonic core. While an increment in shell thickness leads to a decline in local EM intensity and diminished Raman signal, fabricating satellites on the nanoshell can create additional EM "hotspots", improving sensitivity and

detection capabilities. Due to the synergistic benefits, multi-layered hybrid nanostructures such as the layered plasmonic core−shell-satellite (PCSS) configuration has garnered significant attention for applications including biosensing, cancer therapy, and drug delivery.[36]

The inflated cost and susceptibility to issues, such as corrosion, recrystallization, and contamination, make AgNPs less than ideal for SERS applications.[37] Consequently, there is a growing need for cost-efficient robust alternatives, motivating our exploration of noble transition metal as a suitable shell to protect the plasmonic core.[38] This innovative investigation delves into the intricate relationship between transition metal shells and plasmonic nanostructures, particularly Pt and Pd, within the context of PCSS configurations. Traditionally considered nonactive for SERS due to their interband excitation in the visible range causing quenching effects, Pt and Pd's catalytic and electrochemical properties make them intriguing candidates.[39] Theoretical tools, particularly FDTD, are crucial for understanding complex plasmonic and EM interactions in SERS. Despite being underrepresented in publications, these tools hold untapped potential to advance the field.[38] FDTD, known for modeling detailed EM interactions in nanoscale structures, is particularly noteworthy for analyzing PCSS nanostructures in SERS applications.[40] By incorporating classical EM principles, FDTD provides insights into the generation, distribution, and strength of "hotspots", with a focus on nanogap distances between the plasmonic core and satellites, and accounting for frequency-dependent dielectric functions of materials.[41]

Our study reveals that the size and shape-dependent optical properties of the nanostructure conforms to classic plasmonic principles. Using a large Ag core as a template for the ultrathin Pt or Pd shells (<4 nm) not only ensured heightened SERS activity throughout the PCSS nanostructure but also enhanced performance through plasmonic coupling with smaller deposited Ag satellites, through "SERS borrowing activity". Analysis of the electric field distribution and intensity across PCSS shapes (sphere, cuboid, pyramid) revealed that the pyramidal configuration optimizes the EF for PCSS of Ag@Pd@Ag and Ag@Pt@Ag, surpassing the EF of bare plasmonic cores by 3 orders of magnitude. These outcomes underscore PCSS nanostructures as promising candidates for generating abundant and intense "hotspots", offering potential for extremely sensitive and reproducible probe molecule detection. Moreover, the in situ SERS method, facilitated by this substrate, offers a straightforward approach for the detection and monitoring of reactions catalyzed by transition metals.[42] Remarkably, despite the significance of layered PCSS nanostructures, there is a notable gap in the literature concerning EM analysis, specifically exploring transition
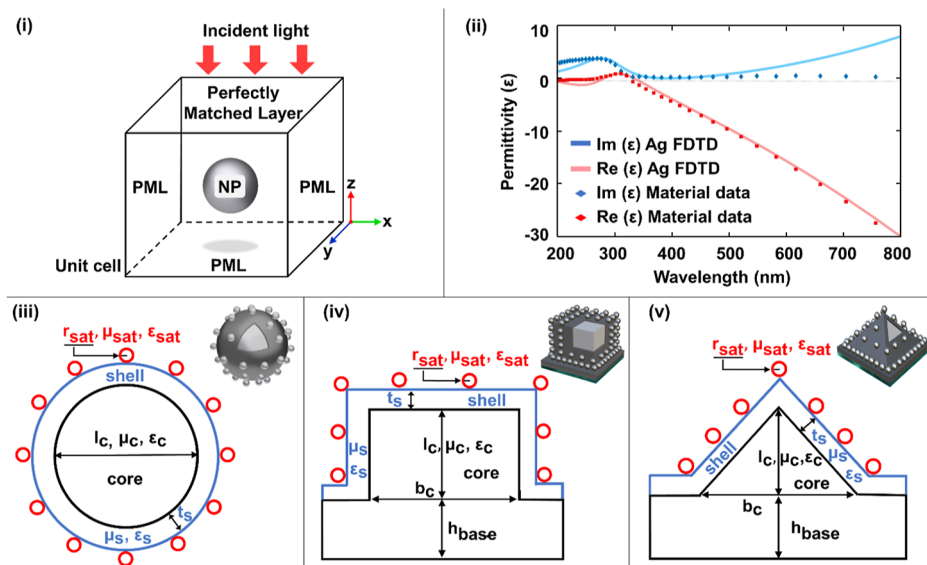
**Figure 2.** (i) FDTD simulation setup and boundary condition for analyzing light scattering phenomenon with nanoparticles (NPs) conducted using ANSYS Lumerical software. (ii) Accuracy comparison between FDTD simulations and material data for the complex permittivity of Ag.[48] Schematic of (iii) spherical, (iv) cuboidal, and (v) pyramidal PCSS designs. The plasmonic core of characteristic length ($l_c$) and breadth ($b_c$) is supported on the base ($h_{base}$) and enveloped by a transition metal shell ($t_s$), serving as a spacer for outer satellites ($r_{sat}$).

metal (Pt/Pd) nanospacers within the layered structures, featuring Ag cores and satellite nanoclusters. This lack of reported studies underscores the novelty of our research, contributing valuable insights into the EM characteristics of these versatile PCSS nanostructures, which hold promise as SERS substrates with broad applicability.

## ■ THEORETICAL METHODOLOGY AND MATERIALS

The theoretical framework employed relies on the discrete spatial and temporal grids known as Yee Cells, introduced in 1966.[43] Within this grid, the electric component is distributed along the edges of the cubic cell, while the magnetic component is situated on the faces. The strength of the local electric field ($|E|_{max}$) expressed as $\frac{\iiint \left|\frac{E}{E_0}\right|^2 dV}{V}$ is derived by calculating the integral volume average of $|E/E_0|^2$ where "$E$" denotes the local maximum of the electric field, "$E_0$" represents the incident amplitude of the light source, and $V$ corresponds to the volume.[44] To avoid nonphysical reflections from the boundaries of the computational domain, perfectly matched layer (PML) boundary conditions are implemented. The PML is defined by the equation

$$E_x^{n+1}(i) - E_x^n(i) = \frac{\Delta t}{\epsilon}\left[\frac{\partial H_z(i)}{\partial y} - \frac{\partial H_y(i)}{\partial z}\right] + \sigma E_x^n(i)$$

Furthermore, for accurately modeling the optical properties of metals, the Lorentz−Drude model is employed, which is given by

$$\epsilon(\omega) = \epsilon_\infty - \frac{\omega_p^2}{\omega^2 + i\gamma\omega}$$

where $\omega_p$ is the plasma frequency, and $\gamma$ is the damping constant.[45,46]

Despite the existence of empirical formulas that rely on parameters like concentration and molecular weight, accurately predicting the enhancement effect proves challenging. This

difficulty stems from the absence of a rigorous theoretical foundation, leading to inconsistent estimations of the SERS EF for the same molecule on a given substrate. Hence, we primarily rely on the assumption that the SERS EF is directly proportional to the fourth power of the electric field enhancement ($|E|_{max}^4$).[47] To ensure reliable simulation outcomes, we maintain a high mesh accuracy of 0.8 nm, with a finer mesh (0.25 nm) applied around metallic features to minimize staircasing effects. Simulation parameters include a 50 fs travel time for a plane-polarized wave in water at 300 K.

For this model, a 3D finite lattice of point dipoles serves as the scatterer, excited by an external field. As seen in Figure 2i, the scattering model employs a total-field scattered-field source, dividing the computational domain into the total field and scattered field regions. A PML is implemented to eliminate boundary reflection influences on calculation results in all structures.[49] Additionally, for cuboid and pyramidal PCSS nanostructures, a periodic boundary layer is applied to model their arrangement in a repeating array accurately.[50] This selection was made based on the substantial enhancement observed only with these two shapes when arranged in an array. Critical emphasis was placed on the accurate simulation of real ($Re$) and imaginary ($Im$) permittivity ($\varepsilon$) of the plasmonic core material, modeled using the Lorentz-Drude dispersion equation, which is consistent with Johnson and Christy's model for Ag.[48,51] The complex permittivity of Ag varies across UV, and visible wavelengths. In the UV, it exhibits low Re ($\varepsilon$) but significant Im ($\varepsilon$) due to strong absorption from surface plasmon excitation. In the visible range, Ag is highly reflective with a negative Re ($\varepsilon$), efficiently reflecting light, and indicating metallic behavior with reduced absorption of visible light.

We employed the Palik model to ascertain the optical constants of Pd and Pt within our PCSS nanostructure. In SERS, the relative permittivity of plasmonic materials significantly influences electric field enhancement. Coating the Ag core with a Pt/Pd shell introduces a material with higher relative permittivity ($\varepsilon_r$), causing a redshift to the LSPR
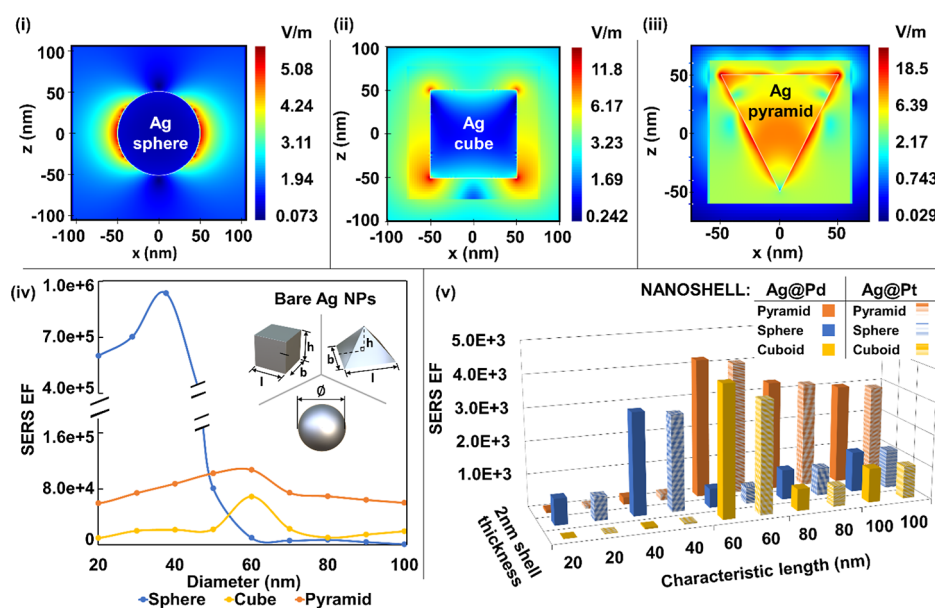
**Figure 3.** Visualization of EM-field intensity distribution ($|E|_{max}$) in the $xz$ plane for 532 nm laser polarized along the $x$ axis for (i) sphere, (ii) cuboid, and (iii) pyramid AgNPs. (iv) Comparative analysis of the shape-dependent optical properties, focusing on the SERS EF ($|E|_{max}^4$), across different shapes. (v) Shape-dependent properties of Ag@Pd and Ag@Pt nanoshells: Exploring "borrowing SERS activity" across various structures with a constant shell thickness of 2 nm.

wavelength. However, the extent of the redshift and the precise tuning of the LSPR wavelength depends on various structural factors as elaborated in Figure 2. These factors include the core size ($l_c$) and geometry, shell thickness ($t_s$), and the dielectric properties of the surrounding medium. The incident light, which is polarized in the $xz$ plane, is simulated using standard visible range wavelengths for Raman scattering (532, 633, and 785 nm). This choice diverges from the usual LSPR range for spherical AgNPs (400−500 nm) due to the presence of a Pt/Pd shell. This shell introduces changes in dielectric properties and LSPR characteristics to longer wavelengths. To simplify the simulation, the incident electric field amplitude is set to 1 V/m.

## PROPOSED SYNTHESIS METHODS

As we look to the future of nanotechnology, the synthesis and scalable production of complex nanostructures such as core−shell-satellite nanoparticles will be increasingly important. In this theoretical discussion, we propose using electrohydrodynamic (EHD) methods to synthesize Ag@Pd@Ag and Ag@Pt@Ag core−shell-satellite NPs, highlighting EHD's advantage for structured arrays.[52]

The process begins with the deposition of an Ag precursor, such as AgNO₃, onto a conductive substrate.[53] The precursor is then reduced to form the Ag NPs that constitute the core layer. A uniform shell of Pd or Pt is applied by introducing metal precursors—PdCl₂ for Pd[54] or PtCl₄²⁻ for Pt[55]—and optimizing electric field parameters to achieve uniform coating.[56] While EHD offers excellent control over core and shell formation, it may not be commonly used for satellite nanoparticle formation, where traditional chemical reduction methods provide better scalability and uniformity,[57] making them more suitable for depositing Ag satellites around the core−shell structures.[58] To enhance environmental sustainability, glycerol[59] can be used as a greener solvent, and environmentally benign reducing agents like ascorbic acid[60] or

sodium citrate[61] can be selected to minimize the environmental impact.

Postprocessing steps, such as annealing, further enhance the stability and optical properties of the nanostructures.[31] This combined approach allows for detailed control over nanoparticle morphology and is well-suited for creating highly structured nanoarrays with applications in catalysis, sensing, and photonics.[62,63,64] With these advancements, EHD methods hold great promise for scaling up production and expanding the potential applications of these nanostructures in future technologies.

## RESULTS AND DISCUSSION

In assessing the SERS effect, factors beyond electric field strength are crucial, including incident and absorbed fields, dipole and quadrupole interactions, photon energy absorption, and inelastic resonant scattering. The observed EF is not solely determined by electric field strength (V/m). Our comprehensive SERS model considers a range of factors, including dielectric medium and object dimensions, computed numerically across the simulated region. In Figure 3, "EF" corresponds to $|E|_{max}^4$, indicating the fourth power of the maximum electric field strength ($|E|_{max}$).[65] This measure simplifies the representation of plasmon enhancement across the domain, aiding in numerical analysis at specific points.

Mie theory suggests that for NP sizes smaller than light waves, only the dipole effect matters.[66] Changes in NP configuration alter the distribution of multipoles, affecting the EM-field. The data in Figure 3 highlights the interplay between size, shape, and SERS activity of AgNPs in PCSS nanostructures. To optimize SERS performance, EM-field distribution and intensity were analyzed for different core shapes (spherical, cuboidal, and pyramidal) at a consistent core size ($l_c$) of 100 nm. The results show varied EM-field intensities: pyramidal NPs ($10^5$) surpass cuboidal NPs ($10^4$) and spherical NPs ($10^2$). This aligns with geometric characteristics; pyramidal NPs, with sharp vertices, create potent EM-
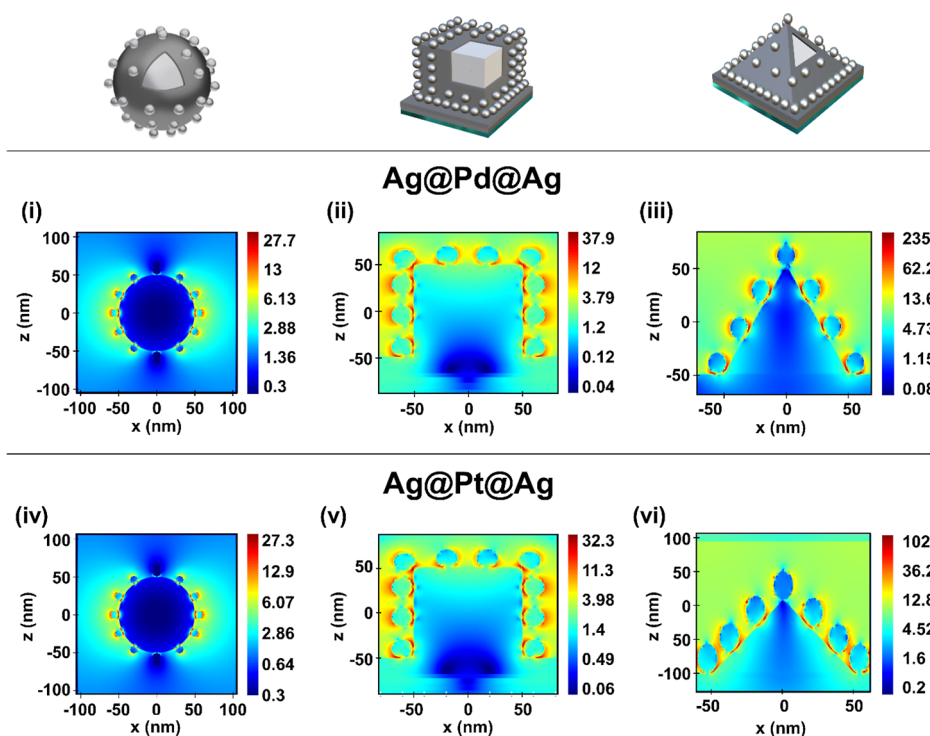
**Figure 4.** Electric field intensity ($|E|_{max}$) and distribution in the $xz$ plane under 532 nm laser for PCSS nanostructures with sphere, cuboid (15 nm $r_{sat}$), and pyramid cores (20 nm $r_{sat}$). For Ag@Pd@Ag (i−iii) and Ag@Pt@Ag (iv-vi). PCSS configuration: 100 nm $l_c$, 3 nm $t_s$, and 20 nm $h_{base}$.

field "hotspots" for stronger SERS effects.[67] Asymmetry and anisotropy in pyramidal NPs widen the spectral absorption and enhance the spectral confinement.[68]

Revealed in Figure 3iv are the unique size-dependent trends in EF and SERS performance for different NP shapes, echoing earlier findings in nanoparticle research. Cuboidal NPs demonstrate size-dependent EF increase but lower SERS activity. Spherical NPs follow classical plasmonic effects, with EF increasing as core size decreases (suitable for small satellites).[69] Pyramidal NPs exhibit significantly higher EF values at larger sizes (ideal for the core).[70] This highlights the impact of NPs shape and size on the theoretical SERS enhancement.

The results in Figure 3v reveal the shape-dependent properties of Ag@Pd and Ag@Pt nanoshells in terms of SERS EF across different characteristic lengths. With a constant shell thickness of 2 nm, the results highlight notable variations in EF across different nanostructures and characteristic lengths. Pyramidal nanostructures consistently exhibit the highest EF values across most dimensions, followed by spheres and cuboids. Interestingly, Ag@Pt nanostructures demonstrate slightly lower EF compared to Ag@Pd nanostructures across all configurations. These insights contribute to a robust PCSS SERS substrate design, with pyramidal structures showing the most promising results for leveraging "borrowing SERS activity" in practical applications. Further exploration of these findings is detailed in Figure 4, providing a comprehensive view of the electric field results.

Figure 4 reveals diverse electric field patterns in nanoshell configurations (sphere, cuboid, and pyramid), indicating that shape and size strongly influence electric field strength. Pyramidal and cuboidal shapes exhibit intense localized "hotspots" due to sharp edges concentrating the electric field, with the pyramid shape standing out for robust SERS

enhancement. The coupling between plasmonic cores and satellites, along with satellite proximity, facilitated by "borrowing SERS activity", significantly shapes the electric field in PCSS structures.[71] The relationship between coverage area and SERS enhancement influences satellite quantity and coupling, with pyramidal and cuboidal shapes reaching peak results at 45% coverage, while spherical cores achieve maximum clustering efficiency with 30%. These insights can guide nanoshell design for optimal SERS enhancement in diverse applications.[72] Analyzing the EF performance in the vis-NIR range, as depicted in Figure 5, is essential for leveraging plasmonic effects, optimizing wavelength tunability, and ensuring broad applicability in various sensing applications.

The introduction of a Pd/Pt shell, characterized by a higher $\varepsilon_r$, results in a shift in observed EF values toward longer wavelengths compared to the typical LSPR range of AgNPs (400 to 500 nm). Figure 5 demonstrates that Ag@Pt@Ag consistently shows elevated EF ($10^5-10^6$) for spherical and cuboidal substrates at 532 nm, decreasing with longer wavelengths. In contrast, the pyramidal core, particularly Ag@Pd@Ag, exhibits remarkably high EF of $10^9$ at 532 nm, surpassing other shapes by 3 orders of magnitude. This underscores its significant potential for robust SERS applications in the visible range. To contextualize our findings, we compared them with recent FDTD simulation studies on diverse SERS substrates (Ag, Pt, or Pd-containing nanostructures). Table 1 summarizes key outcomes from these studies, aligning with our research.

Comparing EF values among different SERS substrates, including Ag, Pt, and Pd in complex nanostructures, Table 1 reveals insights into PCSS nanostructures, highlighting distinctive EF trends under various excitation wavelengths. The findings are compared with recent studies, offering a
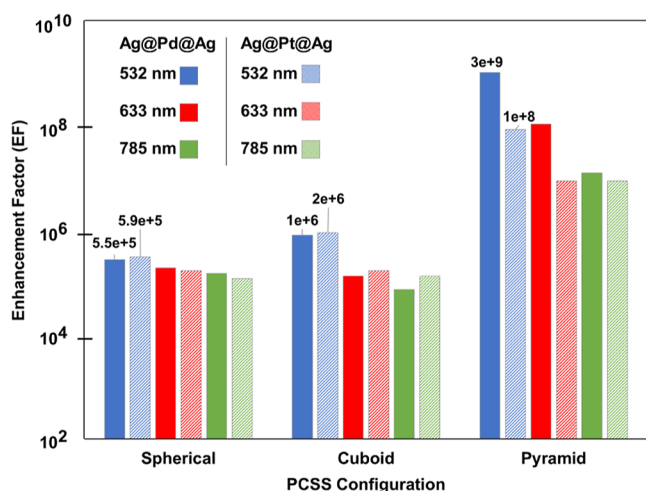
**Figure 5.** Comparison of EF ($|E|^4_{max}$) of PCSS nanostructures with Ag@Pd@Ag and Ag@Pt@Ag configurations under common visible range SERS wavelengths (532, 633, and 785 nm).

comprehensive overview of materials and nanostructures. Notably, Ag@Pd@Ag and Ag@Pt@Ag PCSS configurations exhibit exceptionally high EF ($10^9$ and $10^8$, respectively), outperforming various structures. From nanowires to core–shell configurations, the table illustrates unique EF values, emphasizing the impact of design variations on SERS performance. This comparative analysis serves as a valuable reference for researchers navigating the intricate landscape of SERS substrates.

## CONCLUSION

This study provides a comprehensive exploration of the intricate dynamics within Plasmonic Core–Shell-Satellite (PCSS) configurations, focusing on Pt and Pd-coated Ag cores as robust SERS substrates. Through rigorous FDTD analysis, our numerical modeling revealed the nuanced size and shape-dependent optical properties, emphasizing the critical role of transition metal spacers and nanoclustered satellites. Numerical analysis establishes optimal PCSS configurations with a core size ($l_c$) of 100 nm and a shell thickness ($t_s$) of 3 nm, adorned with Ag-cluster satellites ($r_{sat}$) ranging from 10 to 20 nm for PCSS substrates of Ag@Pd@Ag and Ag@Pt@Ag. Notably, the pyramidal shape demonstrated superior performance, boasting an EF of $10^9$, surpassing its spherical and cuboidal counterparts by 3 orders of magnitude, underscoring the synergetic interactions between the core, shell, and satellite nanostructures. Addressing gaps in transition metal nanospacer analysis within PCSS structures, our findings pave the way for advanced engineering and catalytic applications. While acknowledging that practical limitations may yet be identified through experimental confirmation, our study highlights the significance of theoretical methods in advancing SERS technology, offering valuable insights, and suggesting promising directions for future research in this field.

## AUTHOR INFORMATION

### Corresponding Author

Guogang Ren − Science and Technology Research Institute, University of Hertfordshire, Hatfield, Herts AL10 9AB, U.K.; orcid.org/0000-0001-8865-1526; Email: g.g.ren@herts.ac.uk

### Authors

Patrick Irigo − Science and Technology Research Institute, University of Hertfordshire, Hatfield, Herts AL10 9AB, U.K.
Nada Yousif − Science and Technology Research Institute, University of Hertfordshire, Hatfield, Herts AL10 9AB, U.K.
Ian Johnston − Science and Technology Research Institute, University of Hertfordshire, Hatfield, Herts AL10 9AB, U.K.
Boyan Tatarov − Science and Technology Research Institute, University of Hertfordshire, Hatfield, Herts AL10 9AB, U.K.

**Table 1. Comparative Analysis of FDTD Simulation Results for Diverse SERS Substrates with Complex Nanostructures, Including Ag, Pd, and Pt, in Context with Current Study[a]**

| substrate | nanostructure | fabrication method | enhancement factor (EF) | reference |
|---|---|---|---|---|
| Ag@Pd@Ag | PCSS | self-assembly | $\sim 3 \times 10^9$ | this study |
| Ag@Pt@Ag | PCSS | self-assembly | $\sim 1 \times 10^8$ | this study |
| Ag | nanoplate arrays | electro-deposition | $\sim 1.0 \times 10^9$ | 73 |
| Pt | aggregates | chemical reduction | $\sim 1 \times 10^2$ | 39 |
| Pd | dendrites | chemical reduction | $\sim 1 \times 10^1$ | 39 |
| Ag@Pd | nanowires | femtosecond laser fabrication | $\sim 2.6 \times 10^8$ | 74 |
| Ag@Pt | core−satellite | self-assembly | $\sim 3.5 \times 10^4$ | 75 |
| Au@Pd | core−shell | self-assembly | $\sim 5 \times 10^4$ | 76 |
| Ag@Si | 2.5D NW | template technique; vapor deposition | $\sim 3.2 \times 10^6$ | 77 |
| Ag@Si $O_2$ | Core−shell | seed-mediated method | $\sim 5.7 \times 10^8$ | 41 |
| Ag@SiN | arrays with nm gap | E-beam lithography | $\sim 1 \times 10^9 \sim 10^{10}$ | 78 |
| Ag@$Si_3N_4$ | nanohole arrays | nanoimprint lithography | $\sim 1 \times 10^7$ | 79 |
| Ag@$Al_2O_3$@Ag | PCSS | self-assembly | $\sim 1.7 \times 10^7$ | 31 |
| Ag@$TiO_2$@Ag | PCSS | self-assembly | $\sim 1 \times 10^4$ | 80 |
| Ag−NCs@p-ATP@Pt | Sandwich | self-assembly | $\sim 4 \times 10^6$ | 81 |
| AuSSV@Pt | SSV array | electrodeposition | $\sim 3.7 \times 10^4$ | 82 |
| Si@Pd | nanoflowers: diverse morphologies | electroless deposition | $\sim 1 \times 10^6$ | 83 |
| Ag@AAO@Al | nanostructure arrays | E-beam evaporation technique | $\sim 9.8 \times 10^7$ | 84 |
| Ag@AAO@PC | anemone | template technique | $\sim 1.0 \times 10^{11}$ | 85 |
| Ag@PATP-SAM@Ag | sandwich | self-assembly | $\sim 2.5 \times 10^9$ | 86 |

$^a$Adapted with permission from ref 40 Copyright 2016 Elsevier.

**Avinash Yadav** − *Science and Technology Research Institute, University of Hertfordshire, Hatfield, Herts AL10 9AB, U.K.*

**Etelka Chung** − *Science and Technology Research Institute, University of Hertfordshire, Hatfield, Herts AL10 9AB, U.K.*

**Kun Luo** − *School of Materials Science and Engineering, Changzhou University, Changzhou 213164, China;* ⊙ orcid.org/0000-0001-6526-4304

Complete contact information is available at:
https://pubs.acs.org/10.1021/acs.jpcc.4c05229

## Author Contributions

The manuscript was written through contributions of all authors. All authors have given approval to the final version of the manuscript.

## Notes

The authors declare no competing financial interest.

## ■ ABBREVIATIONS

SERS, surface-enhanced Raman spectroscopy; PCSS, plasmonic core−shell-satellite; FDTD, finite-difference time-domain; EM, electromagnetic; NPs, nanoparticles; LSPR, localized surface Plasmon resonance; EF, enhancement factor; PML, perfectly matched layer; EHD, electrohydrodynamic

## ■ REFERENCES

(1) Moskovits, M. Surface-enhanced spectroscopy. *Rev. Mod. Phys.* **1985**, *57* (3), 783−826.

(2) Huynh, K. H.; Hahm, E.; Noh, M. S.; Lee, J. H.; Pham, X. H.; Lee, S. H.; Kim, J.; Rho, W. Y.; Chang, H.; Kim, D. M.; et al. Recent Advances in Surface-Enhanced Raman Scattering Magnetic Plasmonic Particles for Bioapplications. *Nanomaterials* **2021**, *11* (5), 1215.

(3) Huang, Z.; Zhang, A.; Zhang, Q.; Cui, D. Nanomaterial-based SERS sensing technology for biomedical application. *J. Mater. Chem. B* **2019**, *7* (24), 3755−3774.

(4) Halouzka, V.; Halouzkova, B.; Jirovsky, D.; Hemzal, D.; Ondra, P.; Siranidi, E.; Kontos, A. G.; Falaras, P.; Hrbac, J. Copper nanowire coated carbon fibers as efficient substrates for detecting designer drugs using SERS. *Talanta* **2017**, *165*, 384−390.

(5) Liu, C.; Müller-Böttcher, L.; Liu, C.; Popp, J.; Fischer, D.; Cialla-May, D. Raman-based detection of ciprofloxacin and its degradation in pharmaceutical formulations. *Talanta* **2022**, *250*, 123719.

(6) Yang, D. P.; Chen, S.; Huang, P.; Wang, X.; Jiang, W.; Pandoli, O.; Cui, D. Bacteria-template synthesized silver microspheres with hollow and porous structures as excellent SERS substrate. *Green Chem.* **2010**, *12* (11), 2038−2042.

(7) Sivanesan, A.; Witkowska, E.; Adamkiewicz, W.; Dziewit, Ł.; Kamińska, A.; Waluk, J. Nanostructured silver−gold bimetallic SERS substrates for selective identification of bacteria in human blood. *Analyst* **2014**, *139* (5), 1037−1043.

(8) Rule, K.; Vikesland, P. J. Surface-enhanced resonance raman spectroscopy for the rapid detection of cryptosporidium parvum and giardia lamblia. *Environ. Sci. Technol.* **2009**, *43* (4), 1147−1152.

(9) He, D.; Wu, Z.; Cui, B.; Xu, E.; Jin, Z. Establishment of a dual mode immunochromatographic assay for Campylobacter jejuni detection. *Food Chem.* **2019**, *289*, 708−713.

(10) Muehlethaler, C.; Leona, M.; Lombardi, J. R. Review of Surface Enhanced Raman Scattering Applications in Forensic Science. *Anal. Chem.* **2016**, *88* (1), 152−169.

(11) Asiala, S. M.; Schultz, Z. D. Characterization of hotspots in a highly enhancing SERS substrate. *Analyst* **2011**, *136* (21), 4472−4479.

(12) Otto, A.; Mrozek, I.; Grabhorn, H.; Akemann, W. Surface-enhanced Raman scattering. *J. Phys.: Condens. Matter* **1992**, *4* (5), 1143−1212.

(13) Sui, M.; Kunwar, S.; Pandey, P.; Lee, J. Strongly confined localized surface plasmon resonance (LSPR) bands of Pt, AgPt, AgAuPt nanoparticles. *Sci. Rep.* **2019**, *9* (1), 16582.

(14) Kelly, K. L.; Coronado, E.; Zhao, L. L.; Schatz, G. C. The optical properties of metal nanoparticles: The influence of size, shape, and dielectric environment. *J. Phys. Chem. B* **2003**, *107* (3), 668−677.

(15) Moskovits, M. Surface-enhanced Raman spectroscopy: a brief retrospective. *J. Raman Spectrosc.* **2005**, *36* (6−7), 485−496.

(16) Jayawardhana, S.; Rosa, L.; Juodkazis, S.; Stoddart, P. R. Additional Enhancement of Electric Field in Surface-Enhanced Raman Scattering due to Fresnel Mechanism. *Sci. Rep.* **2013**, *3*, 2335.

(17) Ye, J.; Hutchison, J. A.; Uji-i, H.; Hofkens, J.; Lagae, L.; Maes, G.; Borghs, G.; Van Dorpe, P. Excitation wavelength dependent surface enhanced Raman scattering of 4-aminothiophenol on gold nanorings. *Nanoscale* **2012**, *4* (5), 1606−1611.

(18) Turkevich, J. Colloidal gold. Part II - Colour, coagulation, adhesion, alloying and catalytic properties. *Gold Bull.* **1985**, *18* (4), 125−131.

(19) Le Ru, E. C.; Blackie, E.; Meyer, M.; Etchegoin, P. G. Surface enhanced raman scattering enhancement factors: A comprehensive study. *J. Phys. Chem. C* **2007**, *111* (37), 13794−13803.

(20) Huang, G.; Zhao, H.; Li, P.; Liu, J.; Chen, S.; Ge, M.; Qin, M.; Zhou, G.; Wang, Y.; Li, S.; et al. Construction of Optimal SERS Hotspots Based on Capturing the Spike Receptor-Binding Domain (RBD) of SARS-CoV-2 for Highly Sensitive and Specific Detection by a Fish Model. *Anal. Chem.* **2021**, *93* (48), 16086−16095.

(21) Quan, J.; Zhang, J.; Qi, X.; Li, J.; Wang, N.; Zhu, Y. A study on the correlation between the dewetting temperature of Ag film and SERS intensity. *Sci. Rep.* **2017**, *7* (1), 14771.

(22) Rycenga, M.; Xia, X.; Moran, C. H.; Zhou, F.; Qin, D.; Li, Z.-Y.; Xia, Y.; Rycenga, M.; Xia, X.; Moran, C. H.; et al. Generation of Hot Spots with Silver Nanocubes for Single-Molecule Detection by Surface-Enhanced Raman Scattering. *Angew. Chem., Int. Ed.* **2011**, *50* (24), 5473−5477.

(23) Dai, H.; Fu, P.; Li, Z.; Sun, J.; Fang, H. Electricity mediated plasmonic tip engineering on single Ag nanowire for SERS. *Opt. Express* **2018**, *26* (19), 25031−25036.

(24) Li, S.; Pedano, M. L.; Chang, S. H.; Mirkin, C. A.; Schatz, G. C. Gap structure effects on surface-enhanced raman scattering intensities for gold gapped rods. *Nano Lett.* **2010**, *10* (5), 1722−1727.

(25) Cheng, Y. W.; Wu, C. H.; Chen, W. T.; Liu, T. Y.; Jeng, R. J. Manipulated interparticle gaps of silver nanoparticles by dendron-exfoliated reduced graphene oxide nanohybrids for SERS detection. *Appl. Surf. Sci.* **2019**, *469*, 887−895.

(26) Sharma, V. K.; Yngard, R. A.; Lin, Y. Silver nanoparticles: Green synthesis and their antimicrobial activities. *Adv Colloid Interface Sci.* **2009**, *145*, 83.

(27) Ren, B.; Gao, L.; BotaoXie; Li, M.; Zhang, S.; Zu, G.; Ran, X. Tribological properties and anti-wear mechanism of ZnO@graphene core-shell nanoparticles as lubricant additives. *Tribol. Int.* **2020**, *144*, 106114.

(28) Sanchez, S. I.; Small, M. W.; Zuo, J. M.; Nuzzo, R. G. Structural characterization of Pt-Pd and Pd-Pt core-shell nanoclusters at atomic resolution. *J. Am. Chem. Soc.* **2009**, *131* (24), 8683−8689.

(29) Ding, H. L.; Zhang, Y. X.; Wang, S.; Xu, J. M.; Xu, S. C.; Li, G. H. Fe3O4@SiO2 core/shell nanoparticles: The silica coating

regulations with a single core for different core sizes and shell thicknesses. *Chem. Mater.* **2012**, 24 (23), 4572−4580.

(30) Pastoriza-Santos, I.; Koktysh, D. S.; Mamedov, A. A.; Giersig, M.; Kotov, N. A.; Liz-Marzán, L. M. One-pot synthesis of Ag@TiO2 core-shell nanoparticles and their layer-by-layer assembly. *Langmuir* **2000**, 16 (6), 2731−2735.

(31) Pandey, P.; Kunwar, S.; Shin, K. H.; Seo, M. K.; Yoon, J.; Hong, W. K.; Sohn, J. I. Plasmonic core−shell−satellites with abundant electromagnetic hotspots for highly sensitive and reproducible SERS detection. *Int. J. Mol. Sci.* **2021**, 22 (22), 12191.

(32) Van Duyne, R. P.; Haushalter, J. P.; Janik-Czachor, M.; Levinger, N. Surface-enhanced resonance Raman spectroscopy of adsorbates on semiconductor electrode surfaces. 2. In situ studies of transition metal (iron and ruthenium) complexes on silver/gallium arsenide and silver/silicon. *J. Phys. Chem.* **1985**, 89 (19), 4055−4061.

(33) Wojtysiak, S.; Walczyński, M. S.; Kudelski, A. Silver−platinum core−shell nanoparticles for surface-enhanced Raman spectroscopy. *Vib. Spectrosc.* **2011**, 57 (2), 261−269.

(34) Abu-Surrah, A.; Kettunen, M. Platinum Group Antitumor Chemistry: Design and development of New Anticancer Drugs Complementary to Cisplatin. *Curr. Med. Chem.* **2006**, 13 (11), 1337−1357.

(35) Zhang, Y. J.; Li, S. B.; Duan, S.; Lu, B. A.; Yang, J.; Panneerselvam, R.; Li, C. Y.; Fang, P. P.; Zhou, Z. Y.; Phillips, D. L.; et al. Probing the Electronic Structure of Heterogeneous Metal Interfaces by Transition Metal Shelled Gold Nanoparticle-Enhanced Raman Spectroscopy. *J. Phys. Chem. C* **2016**, 120 (37), 20684−20691.

(36) Deng, Z. J.; Morton, S. W.; Ben-Akiva, E.; Dreaden, E. C.; Shopsowitz, K. E.; Hammond, P. T. Layer-by-layer nanoparticles for systemic codelivery of an anticancer drug and siRNA for potential triple-negative breast cancer treatment. *ACS Nano* **2013**, 7 (11), 9571−9584.

(37) Ishida, T.; Tsuneda, S.; Nishida, N.; Hara, M.; Sasabe, H.; Knoll, W. Surface-Conditioning Effect of Gold Substrates on Octadecanethiol Self-Assembled Monolayer Growth. *Langmuir* **1997**, 13 (17), 4638−4643.

(38) Langer, J.; Jimenez de Aberasturi, D.; Aizpurua, J.; Alvarez-Puebla, R. A.; Auguié, B.; Baumberg, J. J.; Bazan, G. C.; Bell, S. E. J.; Boisen, A.; Brolo, A. G.; et al. Present and future of surface-enhanced Raman scattering. *ACS Nano* **2020**, 14 (1), 28−117.

(39) Tran, M.; Whale, A.; Padalkar, S. Exploring the Efficacy of Platinum and Palladium Nanostructures for Organic Molecule Detection via Raman Spectroscopy. *Sensors* **2018**, 18 (1), 147.

(40) Zeng, Z.; Liu, Y.; Wei, J. Recent advances in surface-enhanced raman spectroscopy (SERS): Finite-difference time-domain (FDTD) method for SERS and sensing applications. *TrAC, Trends Anal. Chem.* **2016**, 75, 162−173.

(41) Uzayisenga, V.; Lin, X. D.; Li, L. M.; Anema, J. R.; Yang, Z. L.; Huang, Y. F.; Lin, H. X.; Li, S. B.; Li, J. F.; Tian, Z. Q. Synthesis, characterization, and 3D-FDTD simulation of Ag@SiO2 nanoparticles for shell-isolated nanoparticle-enhanced raman spectroscopy. *Langmuir* **2012**, 28 (24), 9140−9146.

(42) Zhu, Y.; Tang, H.; Wang, H.; Li, Y. In Situ SERS Monitoring of the Plasmon-Driven Catalytic Reaction by Using Single Ag@Au Nanowires as Substrates. *Anal. Chem.* **2021**, 93 (34), 11736−11744.

(43) Yee, K. S. Numerical Solution of Initial Boundary Value Problems Involving Maxwell's Equations in Isotropic Media. *IEEE Trans. Antennas Propag.* **1966**, 14 (3), 302−307.

(44) Li, J. F.; Huang, Y. F.; Ding, Y.; Yang, Z. L.; Li, S. B.; Zhou, X. S.; Fan, F. R.; Zhang, W.; Zhou, Z. Y.; Wu, D. Y.; et al. Shell-isolated nanoparticle-enhanced Raman spectroscopy. *Nature* **2010**, 464 (7287), 392−395.

(45) Rakić, A. D.; Djurišić, A. B.; Elazar, J. M.; Majewski, M. L. Optical properties of metallic films for vertical-cavity optoelectronic devices. *Appl. Opt.* **1998**, 37 (22), 5271−5283.

(46) Berenger, J. P. A perfectly matched layer for the absorption of electromagnetic waves. *J. Comput. Phys.* **1994**, 114 (2), 185−200.

(47) Wei, H.; Leng, W.; Song, J.; Willner, M. R.; Marr, L. C.; Zhou, W.; Vikesland, P. J. Improved Quantitative SERS Enabled by Surface Plasmon Enhanced Elastic Light Scattering. *Anal. Chem.* **2018**, 90 (5), 3227−3237.

(48) Johnson, P. B.; Christy, R. W. Optical Constants of the Noble Metals. *Phys. Rev. B* **1972**, 6 (12), 4370−4379.

(49) Bérenger, J.-P. *Perfectly Matched Layer (PML) for Computational Electromagnetics*; Morgan & Claypool Publishers, 2007; .

(50) Kogon, A. J.; Sarris, C. D., FDTD Modeling of Periodic Structures: A Review. 2020, arXiv:2007.05091v2. arXiv. https://arxiv.org/abs/2007.05091v2.

(51) Sehmi, H. S.; Langbein, W.; Muljarov, E. A. Optimizing the Drude-Lorentz model for material permittivity: Method, program, and examples for gold, silver, and copper. *Phys. Rev. B* **2017**, 95 (11), 115444.

(52) Meng, Z.; Li, J.; Chen, Y.; Gao, T.; Yu, K.; Gu, B.; Qu, M.; Li, X.; Lan, H.; Li, D.; et al. Micro/nanoscale electrohydrodynamic printing for functional metallic structures. *Mater. Today Nano* **2022**, 20, 100254.

(53) Guo, L.; Tang, H.; Wang, X.; Yuan, Y.; Zhu, C. Nanoporous Ag-Decorated Ag7O8NO3 Micro-Pyramids for Sensitive Surface-Enhanced Raman Scattering Detection. *Chemosensors* **2022**, 10 (12), 539.

(54) Wen, X.; Nazemi, S. A.; da Silva, R. R.; Moth-Poulsen, K. The Effect of the Pd Precursors on the Shape of Hollow Ag-Pd Alloy Nanoparticles Using Ag Nanocubes as Seeds. *Langmuir* **2023**, 39 (32), 11268−11273.

(55) Lu, X.; Luo, F.; Song, H.; Liao, S.; Li, H. Pulse electro-deposition to prepare core−shell structured AuPt@Pd/C catalyst for formic acid fuel cell application. *J. Power Sources* **2014**, 246, 659−666.

(56) Onses, M. S.; Sutanto, E.; Ferreira, P. M.; Alleyne, A. G.; Rogers, J. A. Mechanisms, Capabilities, and Applications of High-Resolution Electrohydrodynamic Jet Printing. *Small* **2015**, 11 (34), 4237−4266.

(57) Chai, Z.; Childress, A.; Busnaina, A. A. Directed Assembly of Nanomaterials for Making Nanoscale Devices and Structures: Mechanisms and Applications. *ACS Nano* **2022**, 16 (11), 17641−17686.

(58) Zakia, M.; Yoo, S. I. Core−satellite assemblies of Au@polydopamine@Ag nanoparticles for photothermal-mediated catalytic reaction. *Soft Matter* **2020**, 16 (45), 10252−10259.

(59) Wang, X. A.; Shen, W.; Zhou, B.; Yu, D.; Tang, X.; Liu, J.; Huang, X. The rationality of using core−shell nanoparticles with embedded internal standards for SERS quantitative analysis based glycerol-assisted 3D hotspots platform. *RSC Adv.* **2021**, 11 (33), 20326−20334.

(60) Murugadoss, A.; Kar, M.; Pasricha, R.; Chattopadhyay, A. Silver fused conducting fiber formation of Au-Ag core-shell nanoparticles mediated by ascorbic acid. *Plasmonics* **2009**, 4 (2), 161−170.

(61) Calagua, A.; Alarcon, H.; Paraguay, F.; Rodriguez, J. Synthesis and Characterization of Bimetallic Gold-Silver Core-Shell Nanoparticles: A Green Approach. *Adv. Nanopart.* **2015**, 04 (04), 116−121.

(62) Gawande, M. B.; Goswami, A.; Asefa, T.; Guo, H.; Biradar, A. V.; Peng, D. L.; Zboril, R.; Varma, R. S. Core−shell nanoparticles: synthesis and applications in catalysis and electrocatalysis. *Chem. Soc. Rev.* **2015**, 44 (21), 7540−7590.

(63) Anandan, V.; Rao, Y. L.; Zhang, G. Nanopillar array structures for enhancing biosensing performance. *Int. J. Nanomed.* **2006**, 1 (1), 73−80.

(64) Lee, S. A.; Yang, J. W.; Choi, S.; Jang, H. W. Nanoscale electrodeposition: Dimension control and 3D conformality. *Exploration* **2021**, 1 (3), 20210012.

(65) *Surface-Enhanced Raman Scattering*; Kneipp, K., Moskovits, M., Kneipp, H., Eds.; Springer, 2006; Vol. 103..

(66) Stratton, J. A. *Electromagnetic Theory*; Wiley-IEEE Press, 2015; pp 106−153.

(67) Lee, D.; Yoon, S. Effect of Nanogap Curvature on SERS: A Finite-Difference Time-Domain Study. *J. Phys. Chem. C* **2016**, 120 (37), 20642−20650.

(68) Liao, P. F.; Wokaun, A. Lightning rod effect in surface enhanced Raman scattering. *J. Chem. Phys.* **1982**, *76* (1), 751−752.

(69) Zeman, E. J.; Schatz, G. C. Electromagnetic Theory Calculations for Spheroids: An Accurate Study of the Particle Size Dependence of SERS and Hyper-Raman Enhancements. *The Jerusalem Symposia on Quantum Chemistry and Biochemistry*; Springer, 1984; 413−424..

(70) Stoerzinger, K. A.; Hasan, W.; Lin, J. Y.; Robles, A.; Odom, T. W. Screening Nanopyramid Assemblies to Optimize Surface Enhanced Raman Scattering. *J. Phys. Chem. Lett.* **2010**, *1* (7), 1046−1050.

(71) Tian, Z. Q.; Ren, B.; Li, J. F.; Yang, Z. L. Expanding generality of surface-enhanced Raman spectroscopy with borrowing SERS activity strategy. *Chem. Commun.* **2007**, No. 34, 3514−3534.

(72) Pazos-Perez, N.; Fitzgerald, J. M.; Giannini, V.; Guerrini, L.; Alvarez-Puebla, R. A. Modular assembly of plasmonic core−satellite structures as highly brilliant SERS-encoded nanoparticles. *Nanoscale Adv.* **2019**, *1* (1), 122−131.

(73) Yang, S.; Slotcavage, D.; Mai, J. D.; Guo, F.; Li, S.; Zhao, Y.; Lei, Y.; Cameron, C. E.; Huang, T. J. Electrochemically created highly surface roughened Ag nanoplate arrays for SERS biosensing applications. *J. Mater. Chem. C* **2014**, *2* (39), 8350−8356.

(74) Ma, Z.-C.; Zhang, Y.-L.; Han, B.; Liu, X.-Q.; Zhang, H.-Z.; Chen, Q.-D.; Sun, H.-B. Femtosecond Laser Direct Writing of Plasmonic Ag/Pd Alloy Nanostructures Enables Flexible Integration of Robust SERS Substrates. *Adv. Mater. Technol.* **2017**, *2* (6), 1600270.

(75) Kim, K.; Lee, H. B.; Choi, J. Y.; Kim, K. L.; Shin, K. S. Surface-enhanced raman scattering of 4-aminobenzenethiol in nanogaps between a planar ag substrate and pt nanoparticles. *J. Phys. Chem. C* **2011**, *115* (27), 13223−13231.

(76) Fang, P. P.; Li, J. F.; Yang, Z. L.; Li, L. M.; Ren, B.; Tian, Z. Q. Optimization of SERS activities of gold nanoparticles and gold-core−palladium-shell nanoparticles by controlling size and shell thickness. *J. Raman Spectrosc.* **2008**, *39* (11), 1679−1687.

(77) Zheng, Y.; Wang, W.; Fu, Q.; Wu, M.; Shayan, K.; Wong, K. M.; Singh, S.; Schober, A.; Schaaf, P.; Lei, Y. Surface-Enhanced Raman Scattering (SERS) Substrate Based on Large-Area Well-Defined Gold Nanoparticle Arrays with High SERS Uniformity and Stability. *Chempluschem* **2014**, *79* (11), 1622−1630.

(78) Theiss, J.; Pavaskar, P.; Echternach, P. M.; Muller, R. E.; Cronin, S. B. Plasmonic nanoparticle arrays with nanometer separation for high-performance SERS substrates. *Nano Lett.* **2010**, *10* (8), 2749−2754.

(79) Kumar, S.; Cherukulappurath, S.; Johnson, T. W.; Oh, S. H. Millimeter-sized suspended plasmonic nanohole arrays for surface-tension-driven flow-through SERS. *Chem. Mater.* **2014**, *26* (22), 6523−6530.

(80) Yang, J.; Zhou, L.; Wang, X. Y.; Song, G.; You, L. J.; Li, J. M. Core-satellite Ag/TiO2/Ag composite nanospheres for multiple SERS applications in solution by a portable Raman spectrometer. *Colloids Surf., A* **2020**, *584*, 124013.

(81) Zhu, S.; Fan, C.; Wang, J.; He, J.; Liang, E.; Chao, M. Surface enhanced Raman scattering of 4-aminothiophenol sandwiched between Ag nanocubes and smooth Pt substrate: The effect of the thickness of Pt film. *J. Appl. Phys.* **2014**, *116* (4), 044312.

(82) Hu, J.; Chen, S.; Johnson, R. P.; Lin, X.; Yang, Z.; Russell, A. E. Surface-enhanced raman scattering on uniform Pd and Pt films: From ill-defined to structured surfaces. *J. Phys. Chem. C* **2013**, *117* (47), 24843−24850.

(83) Roy, A.; Singha, S. S.; Majumder, S.; Singha, A.; Banerjee, S.; Satpati, B. Electroless Deposition of Pd Nanostructures for Multifunctional Applications as Surface-Enhanced Raman Scattering Substrates and Electrochemical Nonenzymatic Sensors. *ACS Appl. Nano Mater.* **2019**, *2* (4), 2503−2514.

(84) Yu, X.; Tao, J.; Shen, Y.; Liang, G.; Liu, T.; Zhang, Y.; Wang, Q. J. A metal−dielectric−graphene sandwich for surface enhanced Raman spectroscopy. *Nanoscale* **2014**, *6* (17), 9925−9929.

(85) Daglar, B.; Demirel, G. B.; Khudiyev, T.; Dogan, T.; Tobail, O.; Altuntas, S.; Buyukserin, F.; Bayindir, M. Anemone-like nanostructures for non-lithographic, reproducible, large-area, and ultra-sensitive SERS substrates. *Nanoscale* **2014**, *6* (21), 12710−12717.

(86) Futamata, M. *Highly-Sensitive ATR Raman Spectroscopy Using Surface-Plasmon-Polariton: Infrared and Raman Discussion Group*. Accessed: Oct. 16, 2023. https://www.irdg.org/ijvs/ijvs-volume-4-edition-2/highly-sensitive-atr-raman-spectroscopy-using-surface-plasmon-polariton.